Extinction of quasiparticle interference in underdoped cuprates with coexisting order

Brian M. Andersen[1] and P. J. Hirschfeld[2]
[1]*Niels Bohr Institute, University of Copenhagen, Universitetsparken 5, DK-2100 Copenhagen, Denmark*
[2]*Department of Physics, University of Florida, Gainesville, Florida 32611-8440, USA*
(Received 24 November 2008; revised manuscript received 3 March 2009; published 20 April 2009)

Scanning tunneling spectroscopy (STS) measurements [Y. Kohsaka *et al.*, Nature (London) **454**, 1072 (2008)] have shown that dispersing quasiparticle interference (QPI) peaks in Fourier-transformed conductance maps disappear as the bias voltage exceeds a certain threshold corresponding to the coincidence of the contour of constant quasiparticle energy with the period-doubled (e.g., antiferromagnetic) zone boundary. Here we show that this may be caused by coexisting order present in the *d*-wave superconducting phase. We show explicitly how QPI peaks are extinguished in the situation with coexisting long-range spin-density wave order and discuss the connection with the more realistic case where short-range order is created by quenched disorder. Since it is the localized QPI peaks rather than the underlying antinodal states themselves which are destroyed at a critical bias, our proposal resolves a conflict between STS and photoemission spectroscopy regarding the nature of these states. We also study the momentum-summed density of states in the coexisting phase and show how the competing order produces a kink inside the "V"-shaped *d*-wave superconducting gap in agreement with recent STS measurements [J. W. Alldredge *et al.*, Nat. Phys. **4**, 319 (2008)].

DOI: 10.1103/PhysRevB.79.144515 PACS number(s): 74.20.−z, 74.25.Jb, 74.50.+r, 74.72.−h

I. INTRODUCTION

The understanding of how a Mott insulator with localized states becomes a metal as one gradually increases the carrier concentration remains one of the main challenges of condensed-matter physics. This question may be intimately connected with the so-called nodal-antinodal dichotomy (sharp quasiparticles in the nodal region versus broad, gapped antinodal "quasiparticles") observed by angular resolved photoemission spectroscopy (ARPES) on underdoped cuprate materials.[1,2] Tunneling spectroscopy has also been used to probe states in different regions of momentum space by the help of Fourier transform scanning tunneling spectroscopy (FT-STS).[3–8] In particular, it has been argued that the apparent incoherent antinodal states have their origin in the emergence of charge-ordered regions in the underdoped regime.[7]

In the *d*-wave superconducting (dSC) state near optimal doping, quasiparticle interference observed by FT-STS is dominated by peaks at well-defined wave vectors $\mathbf{q}_i$ which agree well with those predicted by the so-called octet model.[3,7,9] The contours of constant energy (CCE) of the Bogoliubov quasiparticle dispersion are generally shaped like curved ellipses ("bananas") centered at the nodal points; seven different nonzero wave vectors $\mathbf{q}_i$ connect the tips of these bananas. The dispersion of the peaks at $\mathbf{q}_i$ allows one to extract the shape of the underlying Fermi surface[10] as well as the momentum dependence of the superconducting energy gap.[3] A quantitative understanding of the amplitude and width of the peaks, however, is not straightforward to obtain and depends rather sensitively on the nature of the scattering medium. A pointlike scatterer, for example, in an otherwise homogeneous dSC leads to quasiparticle interference (QPI) patterns of both spotlike and arclike dispersive features close to $\mathbf{q}_i$ in the FT-STS images[9,11–15] whereas experimental data appear mostly spotlike. Furthermore, the weights of the various peaks calculated in simple theories differ from experiment. There have been several theoretical attempts to remedy this situation by including more realistic models for the disorder present in $Bi_2Sr_2CaCu_2O_{8+\delta}$ (BSCCO). In particular, as realized recently, it appears important to include the gap inhomogeneity arising from the dopant atoms.[16–21] Models have also included the extended Coulomb potential arising in this material from partly screened $Bi \leftrightarrow Sr$ substitutional disorder and the oxygen dopant atoms.[19] Nevertheless, a complete quantitative description of the FT-STS patterns in the superconducting state is still lacking.

FT-STS has also been used to probe the pseudogap state in the underdoped regime where nondispersive (bias-independent) quasiperiodic conductance modulations have been identified both in BSCCO (Refs. 4, 6–8, and 22) and $Ca_{2-x}Na_xCuO_2Cl_2$ (Na-CCOC).[23] The origin of these peaks remains unknown at present but may be caused by short-range charge order, possibly connected to the existence of nested segments of the Fermi surface near the antinodal regions of the Brillouin zone.[24] In BSCCO near optimal doping nondispersive peaks have also been discussed in terms of pinned and disorder-induced charge orders.[25–29] In Na-CCOC it has been proposed that phonons play a crucial role in stabilizing a *d*-wave charge-density wave order[30] or a surface transition to a commensurate charge-density wave state.[31] At present, however, it remains controversial whether true charge ordering is required for describing the nondispersive local density of states (LDOS) modulations.[32–34]

Recently, new developments in the FT-STS technique allowed for further detailed exploration of the electronic properties of underdoped Na-CCOC and BSCCO. For example, it was argued that tip-elevation errors can be avoided by studying the conductance ratio $Z(\mathbf{r},E=eV)=g(\mathbf{r},V)/g(\mathbf{r},-V)$, where V is the bias voltage and g the conductance, and the detailed properties of the LDOS modulations were investigated in this regime as well.[35–37] It was found that irrespective of the doping level, an "extinction line" exists in momentum space, beyond which most of the dispersing FT-STS peaks ($\mathbf{q}_2,\mathbf{q}_3,\mathbf{q}_6,\mathbf{q}_7$) disappear, to be replaced by a reduced

set $(\mathbf{q}_1^*, \mathbf{q}_5^*)$ of roughly nondispersive peaks.[36] This extinction line is doping independent and coincides with the antiferromagnetic (AF) zone boundary [lines joining the points $(0, \pm\pi)$ and $(\pm\pi, 0)$]. At energies below the scale Δ_0 where the CCE first touches the AF zone boundary, the FT-STS response is similar to the dispersing Bogoliubov quasiparticles obeying the octet model. At energies above Δ_0, the response becomes highly spatially inhomogeneous.

One popular picture of the nodal-antinodal dichotomy invokes intense scattering with momentum transfer near (π, π) which broadens states near the antinodal points. The problem with this picture in the superconducting state, however, is that the phase space for scattering is smallest at precisely these points of momentum space because the *d*-wave gap is largest there. Graser *et al.*[38] calculated the spin-fluctuation spectrum within a random-phase approximation (RPA) formalism and used it to determine the lifetime of states near the node and antinode of a dSC phase. This same framework produces a good description of the resonant magnetic response near (π, π) as measured by neutron scattering.[39] Nevertheless their results, which were consistent with earlier work on quasiparticle lifetimes,[40–42] imply that inelastic scattering of the conventional itinerant spin-fluctuation type cannot severely broaden quasiparticle states in the superconducting state with momenta near the antinodes. This is of course consistent with ARPES experiments, which find broad but well-defined antinodal peaks in the superconducting state of BSCCO.[1,43,44] An important aspect which is left out of the conventional spin-fluctuation scattering analysis, however, is the possibility of additional coexisting order in the underdoped regime. Static stripe order has been observed in several high-T_c materials and appears especially pronounced near 1/8 doping;[45] in the $La_{2-x}Ba_xCuO_4$ (LBCO) system, for example, charge order appears around 50 K and persists to lower temperatures, where it coexists with spin order.[46] In addition, μSR has consistently reported so-called "cluster spin glass" (CSG) signatures of frozen magnetic order throughout the underdoped cuprate phase diagram of $La_{2-x}Sr_xCuO_4$ (LSCO) and BSCCO,[47,48] generally attributed to disorder present in significant amounts due to the dopant atoms. In both LSCO and BSCCO, the nodal-antinodal dichotomy is also observed in ARPES measurements.[49] These observations suggest that quasiparticle scattering from short-range coexisting order may play an important role in explaining the extinction of the QPI peaks in the experiment by Kohsaka *et al.*[36]

At present, there is no consensus on the origin of competing ordering phenomena in the underdoped regime of the cuprates. One general notion is that disorder can pin fluctuating order while still reflecting the intrinsic correlations of the pure system.[50] Several concrete models of pinned fluctuating stripes have been proposed[51–56,77] which resemble experiment in qualitative ways. Another starting point to understand the CSG phase assumes that dopants nucleate droplets of staggered order, which then interfere constructively to create quasi-long-range order.[52,56,57] Models of a disordered spin-density wave (SDW) phase coexisting with *d*-wave pairs can reproduce a number of known experimental results: the magnetic correlations have been shown to protect the nodal quasiparticles,[58,59] reproduce the Fermi arcs and nodal-antinodal dichotomy,[60] as well as the temperature dependence of the superfluid density[58] and thermal conductivity.[59,61] However, at present it remains controversial whether a CSG phase coexisting with preformed Cooper pairs constitutes a proper description of the pseudogap phase or other types of ordering phenomena occur instead or in addition.[30,62–64]

Here we explore the role of competing order on the quasiparticle interference patterns and the momentum-summed density of states in a coexisting phase of long-range ordered SDW and dSC. Although the SDW order in underdoped cuprates generally exists in a glassy state and hence is short range, we know from neutron measurements on underdoped LSCO (Ref. 65) that correlation lengths can be quite long; on the order of 100 lattice spacings. It may therefore be a reasonable starting point to assume a long-range ordered SDW state. In the following this constitutes our starting assumption and we will investigate its consequences for the LDOS modulations. Even though the underdoped materials which exhibit magnetic ordering are characterized by an incommensurate spin-density wave [with Bragg peaks slightly away from (π, π)], we assume (π, π) ordering for simplicity. We note that a related study with focus on the spectral gap has been recently reported in Ref. 66. Below, we focus on the origin of the extinction line and not the high-energy nondispersive LDOS modulations which can be reproduced, for example, by including the charge ordering of the stripe phase.[13] We suggest that the extinction line is a direct manifestation of the competing SDW order and show also how subgap features in the momentum-summed density of states arise as a natural consequence of the SDW order in the coexisting phase. We propose that this is the origin of the kink inside the conventional "V"-shaped *d*-wave gap observed by Alldredge *et al.*[67] in underdoped BSCCO samples. In order to clearly elucidate the role of the SDW order we consider for simplicity a single pointlike potential scatterer. As is well known, other sources of disorder (e.g., pairing disorder) and more realistic real-space scattering centers are important in attempts of quantitative fits to the QPI maps.[19–21] In the following, we focus on simple effects of the SDW order on the QPI patterns; the results should be important for understanding future FT-STS modeling using more realistic disorder configurations.[68]

II. FORMALISM

The FT-STS signal of a disordered dSC has been discussed rather extensively by theoretical models.[9,11–15] In the present case of coexisting SDW order, the translational symmetry is broken and the formalism is very similar to the *d*-density wave approach discussed in Ref. 69. The Hamiltonian reads

$$H = \sum_{\mathbf{k}\sigma} [\epsilon(\mathbf{k}) - \mu] c^\dagger_{\mathbf{k}\sigma} c_{\mathbf{k}\sigma} + \sum_{\mathbf{k}} \left[\sum_{\sigma} \sigma M c^\dagger_{\mathbf{k}+\mathbf{Q}\sigma} c_{\mathbf{k}\sigma} + \Delta(\mathbf{k}) c^\dagger_{\mathbf{k}\uparrow} c^\dagger_{-\mathbf{k}\downarrow} \right] + \text{H.c.}, \quad (1)$$

where $c^\dagger_{\mathbf{k}\sigma}$ creates an electron with momentum $\mathbf{k}$ and spin σ,

M is the SDW order parameter, and $\mathbf{Q}=(\pi,\pi)$ is the (antiferromagnetic) ordering vector. We work in units where the lattice constant $a=1$. The superconducting d-wave gap function is $\Delta(\mathbf{k})=\Delta(\cos k_x-\cos k_y)/2$ and the quasiparticle dispersion is $\epsilon(\mathbf{k})=\epsilon_1(\mathbf{k})+\epsilon_2(\mathbf{k})$, where $\epsilon_1(\mathbf{k})=-2t(\cos k_x+\cos k_y)$ and $\epsilon_2(\mathbf{k})=-4t'\cos k_x \cos k_y-2t''(\cos 2k_x+\cos 2k_y)$. It is convenient to write the normal-state band in this form due to the different symmetry properties of $\epsilon_1(\mathbf{k})$ and $\epsilon_2(\mathbf{k})$ with respect to momentum shifts of the SDW ordering vector $\mathbf{Q}$; $\epsilon_1(\mathbf{k}+\mathbf{Q})=-\epsilon_1(\mathbf{k})$ and $\epsilon_2(\mathbf{k}+\mathbf{Q})=\epsilon_2(\mathbf{k})$. In terms of the following generalized Nambu spinor $\psi_{\mathbf{k}}^{\dagger}=\{c_{\mathbf{k}\uparrow}^{\dagger},c_{\mathbf{k}+\mathbf{Q}\uparrow}^{\dagger},c_{-\mathbf{k}\downarrow},c_{-\mathbf{k}-\mathbf{Q}\downarrow}\}$, we can write the Hamiltonian in the form

$$H=\sum_{\mathbf{k}}\psi_{\mathbf{k}}^{\dagger}A(\mathbf{k})\psi_{\mathbf{k}}, \tag{2}$$

where the sum is restricted to the reduced Brillouin zone (RBZ), $|k_x|+|k_y|\leq\pi$, and $A(\mathbf{k})$ is given by

$$A(\mathbf{k})=\begin{pmatrix}\epsilon_1(\mathbf{k})+\epsilon_2(\mathbf{k})-\mu & M & \Delta(\mathbf{k}) & 0\\ M & -\epsilon_1(\mathbf{k})+\epsilon_2(\mathbf{k})-\mu & 0 & -\Delta(\mathbf{k})\\ \Delta^*(\mathbf{k}) & 0 & -\epsilon_1(\mathbf{k})-\epsilon_2(\mathbf{k})+\mu & M\\ 0 & -\Delta^*(\mathbf{k}) & M & \epsilon_1(\mathbf{k})-\epsilon_2(\mathbf{k})+\mu\end{pmatrix}. \tag{3}$$

The eigenvalues $\pm E_{1,2}(\mathbf{k})$ of $A(\mathbf{k})$ are given by

$$E_{1,2}(\mathbf{k})=\sqrt{([\epsilon_2(\mathbf{k})-\mu]\pm\sqrt{\epsilon_1^2(\mathbf{k})+M^2})^2+\Delta^2(\mathbf{k})}, \tag{4}$$

which for $\Delta(\mathbf{k})=0$ reduces to $E_M^{\pm}(\mathbf{k})=[\epsilon_2(\mathbf{k})-\mu]\pm\sqrt{\epsilon_1^2(\mathbf{k})+M^2}$ and for $M=0$ reduces to $E(\mathbf{k})=\pm\sqrt{[\epsilon_1(\mathbf{k})+\epsilon_2(\mathbf{k})-\mu]^2+\Delta^2(\mathbf{k})}$. The Green's function $G_0(\mathbf{k},i\omega_n)$ of the pure system is obtained from the equation

$$G_0(\mathbf{k},i\omega_n)^{-1}=i\omega_n I-A(\mathbf{k}), \tag{5}$$

where I denotes the 4×4 identity matrix.

In the presence of an impurity term

$$H_{\mathrm{imp}}=\sum_{\mathbf{k},\mathbf{k}'\in\mathrm{RBZ}}\psi_{\mathbf{k}}^{\dagger}V(\mathbf{k},\mathbf{k}')\psi_{\mathbf{k}'}, \tag{6}$$

the impurity contribution to the full Green's function $G(\mathbf{k},\mathbf{k}',i\omega_n)$ is given by

$$G(\mathbf{k},\mathbf{k}',i\omega_n)=G_0(\mathbf{k},i\omega_n)T(\mathbf{k},\mathbf{k}',i\omega_n)G_0(\mathbf{k}',i\omega_n), \tag{7}$$

where

$$T(\mathbf{k},\mathbf{k}',i\omega_n)=V(\mathbf{k},\mathbf{k}')+\sum_{\mathbf{k}''\in\mathrm{RBZ}}V(\mathbf{k},\mathbf{k}'')G_0(\mathbf{k}'',i\omega_n)\times T(\mathbf{k}'',\mathbf{k}',i\omega_n). \tag{8}$$

For a pointlike impurity $V(\mathbf{k},\mathbf{k}')$ [and $T(\mathbf{k},\mathbf{k}',i\omega_n)$] becomes independent of $\mathbf{k}$ and $\mathbf{k}'$. Specifically, a nonmagnetic δ-function scatterer takes the form

$$V(\mathbf{k},\mathbf{k}')=V\begin{pmatrix}1 & 1 & 0 & 0\\ 1 & 1 & 0 & 0\\ 0 & 0 & -1 & -1\\ 0 & 0 & -1 & -1\end{pmatrix}. \tag{9}$$

The change in the LDOS from the pure phase $\delta N(\mathbf{q},\omega)$ is given by[69]

$$\delta N(\mathbf{q},\omega)=\frac{i}{2\pi}\sum_{\mathbf{k}\in\mathrm{RBZ}}g(\mathbf{k},\mathbf{q},\omega), \tag{10}$$

where $g(\mathbf{k},\mathbf{q},\omega)$ is defined as follows. Let $\mathbf{k}'=\mathbf{k}+\mathbf{q}$. If $\mathbf{k}'$ is in the RBZ, then

$$g(\mathbf{k},\mathbf{q},\omega)=\sum_{i=1}^{4}[G_{ii}(\mathbf{k},\mathbf{k}',s_i\omega)-G_{ii}^*(\mathbf{k}',\mathbf{k},s_i\omega)], \tag{11}$$

where $s_i=1$ for the particle-hole sector $i=1,2$ and $s_i=-1$ for the hole-particle sector $i=3,4$. If $\mathbf{k}'$ is not in the RBZ, then define $\mathbf{k}''=\mathbf{k}+\mathbf{q}-\mathbf{Q}$. For this case

$$g(\mathbf{k},\mathbf{q},\omega)=\sum_{i=1,3}[G_{i,i+1}(\mathbf{k},\mathbf{k}'',s_i\omega)-G_{i,i+1}^*(\mathbf{k}'',\mathbf{k},s_i\omega)+G_{i+1,i}(\mathbf{k},\mathbf{k}'',s_i\omega)-G_{i+1,i}^*(\mathbf{k}'',\mathbf{k},s_i\omega)]. \tag{12}$$

Here, $G(\mathbf{k},\mathbf{k}',\omega)$ is obtained by usual analytical continuation $i\omega_n\rightarrow\omega+i0^+$ of $G(\mathbf{k},\mathbf{k}',i\omega_n)$. Below we introduce a finite lifetime broadening $\eta=0.01t$ such that $i\omega_n\rightarrow\omega+i\eta$ and the summation over the RBZ is performed using a 800×800 mesh.

We use a band dispersion with $t=1.0$, $t'=-0.4$, $t''=0.1$, and $\mu=-1.0$, which yields the normal-state Fermi surface shown in Fig. 1. Throughout this paper we set $\Delta=0.3t$ in the superconducting state, yielding an antinodal gap around 50 meV (using $t=150$ meV) which is realistic for underdoped BSCCO. In the following we focus the discussion on energies below this gap energy. We use a single-site impurity potential $V=0.1t$ which is weak in the sense that it does not produce any low energy resonant states.[70,71] Note that the agreement of the simplest such single-impurity theoretical QPI maps with experiment, even in the optimally doped dSC state, is not particularly impressive. In general, such maps exhibit one or two pointlike dispersing features similar to experiments, but otherwise display dispersing arclike features instead of the observed $\mathbf{q}$ spots, as well as many features which are simply not observed. It is thought that better

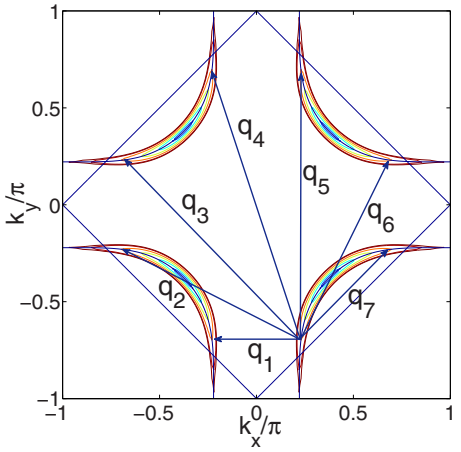

FIG. 1. (Color online) Contours of constant quasiparticle energy for the pure d-wave superconductor with $\Delta=0.3t$ at energies $\omega/\Delta=0.17,0.33,0.50,0.66,0.83,0.90$. Also shown are the underlying normal-state Fermi surface, the RBZ boundary, and the seven distinct nonzero wave vectors $\mathbf{q}_i$ connecting the banana tips.

agreement with experiment can be obtained by including finite range of disorder, pairing disorder, and nonzero density of impurities.[19] Rather than introduce a multitude of parameters to describe such effects, however, in this work we attempt to demonstrate the existence of the qualitative QPI extinction phenomenon, for which it suffices to look at a single potential scatterer. Also for simplicity, we ignore any spatial structure of the local Wannier orbitals, rendering all results periodic in momentum space with respect to reciprocal-lattice vectors. Including spatial structure of the local orbitals[20] and/or extended impurity potentials,[19] both strongly suppress the large-$\mathbf{q}$ features of the QPI maps in qualitative agreement with experiment. Below we do not attempt a quantitative fit to experiments, but focus on the generic features of QPI in the presence of coexisting SDW order.

III. SUPERCONDUCTING PHASE

A detailed discussion of QPI patterns in the pure dSC phase can be found in the literature.[9,11–15,19] However, in order to discuss the effect of competing order on the QPI, we discuss briefly some results for the pure dSC phase in this section. Figure 1 displays typical CCEs exhibiting the usual banana-shaped form, centered at the nodal points $(\pm 0.38, \pm 0.38)\pi$. The wave vectors $\mathbf{q}_i$ connecting the tips of these bananas reveal where peaks in the FT-STS maps are expected, although matrix elements consisting of certain combinations of coherence factors are important for this simple picture to hold.[9,12] Here we calculate the Fourier transform density of states $|\delta N(\mathbf{q},\omega)|$ with $\delta N(\mathbf{q},\omega)$ given by Eq. (10) and refer to it as a QPI map. Figure 2 shows QPI maps versus q_x and q_y at representative fixed energies inside the gap. For clarity, we have circled the $\mathbf{q}_7$ peak which is positioned along the (110) direction and disperses to higher momenta with increasing energy as expected from Fig. 1. We focus on the $\mathbf{q}_7$ peak merely because it remains easily identifiable at all energies below the gap. Other scattering channels can enhance other of the octet vectors.[19] Line cuts along the nodal and antinodal directions for the pure dSC phase are shown in Fig. 3 for both positive and negative energies, exhibiting clearly the dispersive QPI peaks discussed in the literature. The dispersion agrees well with the octet model,[3] which assumes that the scattering peaks are determined entirely by the wave vectors $\mathbf{q}_i$ connecting the banana tips. For example, in Figs. 3(a) and 3(b) one can readily identify the $\mathbf{q}_3$ and $\mathbf{q}_7$ peaks which both disperse to higher momenta with increasing energy. In Fig. 3(b) one can also see the so-called $\mathbf{q}'$ peak near $q_x/\pi=0.76$ arising from internode scattering.[13] Along the (100) direction the FT-STS response is weaker at low energies as seen in Figs. 3(c) and 3(d) but it is still possible to identify both the $\mathbf{q}_1$ and $\mathbf{q}_5$ peaks which disperse to lower and higher momenta with increasing energy, respectively.

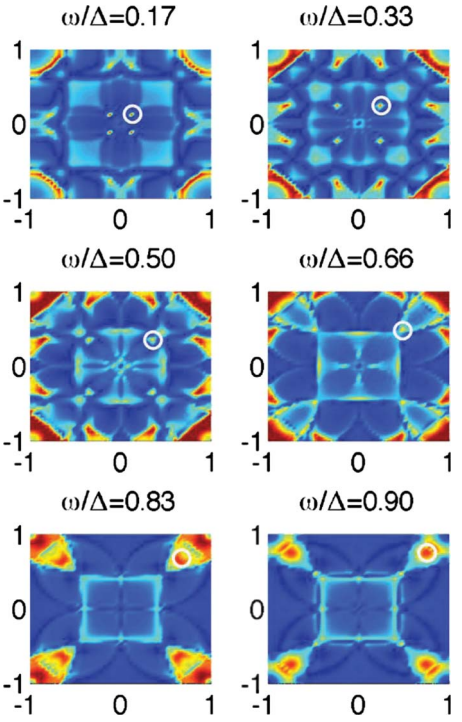

FIG. 2. (Color online) QPI maps vs q_x/π and q_y/π in the dSC phase in the presence of single pointlike potential scatterer of strength $V=0.1t$. Energies ω are as shown in the figure titles. Dispersing spotlike features corresponding to some of the octet vectors $\mathbf{q}_i$ are easy to identify. For example, we have circled the intrabanana $\mathbf{q}_7$ peak (see Fig. 1).

IV. SPIN-DENSITY WAVE PHASE

As discussed in Sec. I there is experimental evidence that in underdoped cuprates SDW order exists in a glassy or slowly fluctuating state. In this section we discuss the simpler case of a homogeneous long-range-ordered metallic SDW phase. Clearly such a phase by itself is too simplistic to describe the pseudogap phase, but it is still important to identify its generic fingerprints in the spectral weight and QPI patterns.

In the pure dSC state, the spectral weight at the Fermi energy $A(\mathbf{k},\omega=0)$ consists of four nodal points, which may

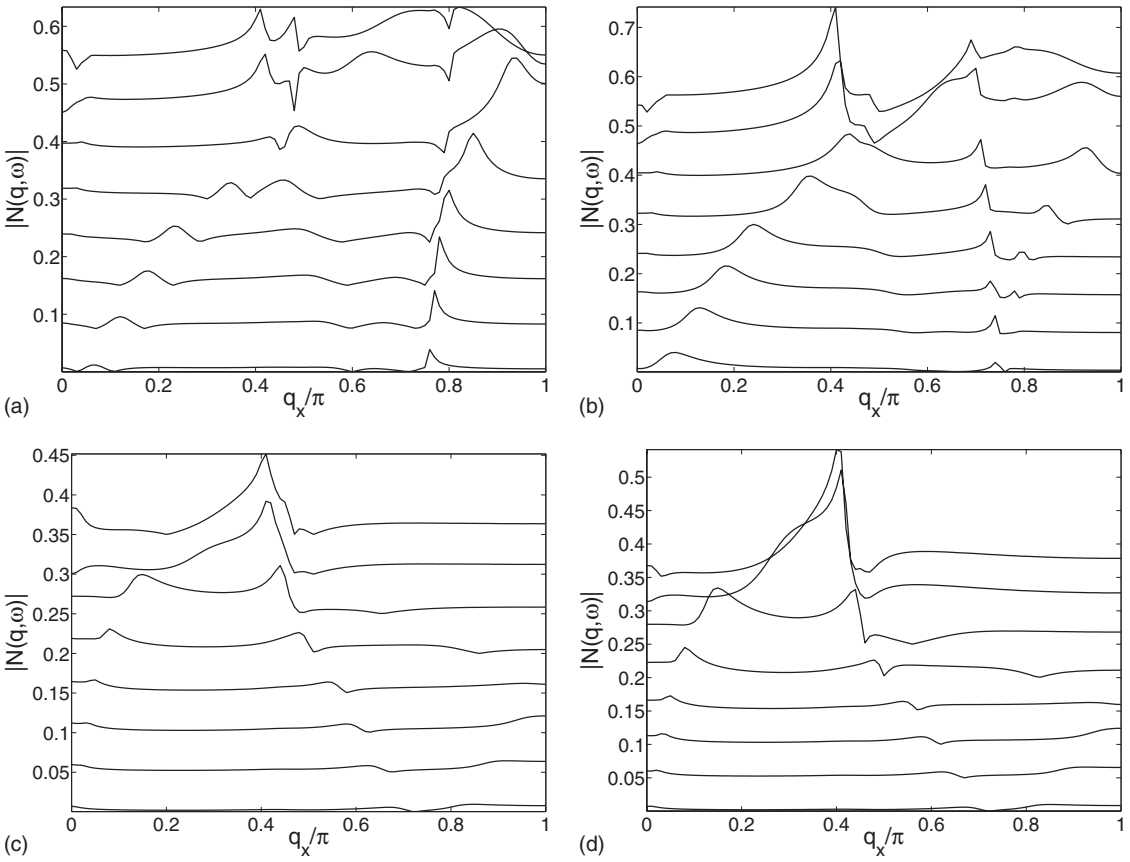

FIG. 3. QPI line cuts along the [(a) and (b)] (110) and [(c) and (d)] (100) directions for the pure dSC phase. Panels (a) and (c) [(b) and (d)] correspond to positive (negative) energies at $|\omega|/\Delta = 0.08, 0.17, 0.25, 0.33, 0.5, 0.66, 0.83, 0.9$ (bottom to top). For clarity the (110) [(100)] curves are displaced by 0.075 (0.05).

be smeared slightly by disorder. In the pure SDW case, the spectral function can be written as

$$A(\mathbf{k},\omega) = v^2(\mathbf{k})\delta[\omega - E_M^-(\mathbf{k})] + u^2(\mathbf{k})\delta[\omega - E_M^+(\mathbf{k})], \tag{13}$$

with $u^2(\mathbf{k}) = 1/2[1 + \epsilon_1(\mathbf{k})/\sqrt{M^2 + \epsilon_1^2(\mathbf{k})}]$ and $v^2(\mathbf{k}) = 1/2[1 - \epsilon_1(\mathbf{k})/\sqrt{M^2 + \epsilon_1^2(\mathbf{k})}]$. In Figs. 4(a) and 4(b) we show the spectral weight $A(\mathbf{k}, \omega = 0)$ in the metallic case with $M = 0.5t$ (a) and $M = t$ (b). From Fig. 4(a) one sees that $M = 0.5t$ is still rather weak in the sense that spectral weight remains near the antinodal regions. Furthermore, as seen in both Figs. 4(a) and 4(b), the intensity of the outer ring of the Fermi pocket tends to be strongly reduced, which is caused by the $v^2(\mathbf{k})$ coherence factor. This is a simple consequence of the unit cell doubling in the SDW state and a similar effect happens in, e.g., the *d*-density wave scenario.[72] The checkerboard charge-order scenario for the pseudogap phase also reproduces a Fermi arc due to the difference in the coherence factors between the inner and outer parts of the arc.[30,62] A disordered SDW will further enhance the spectral weight suppression on the outside of the pockets.[73]

Figures 4(c) and 4(d) show typical CCEs in the metallic SDW phase. For positive energies $\omega > 0$ the pockets centered at the nodal (antinodal) region shrink (expand) with increasing energy. The opposite behavior is valid for $\omega < 0$ display-

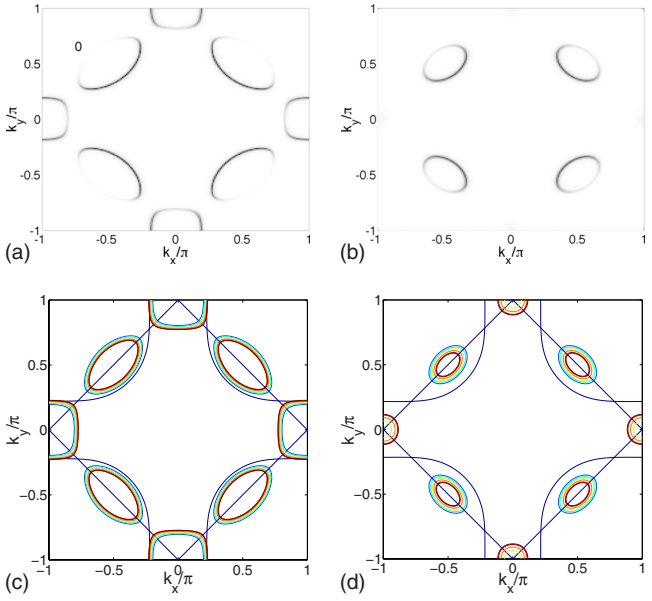

FIG. 4. (Color online) Spectral weight $A(\mathbf{k}, \omega = 0)$ in the pure SDW phase with (a) $M = 0.5t$ and (b) $M = t$. Lower two panels (c) and (d) show CCEs at the same energies as in Fig. 1 for (c) $M = 0.5t$ and (d) $M = t$.

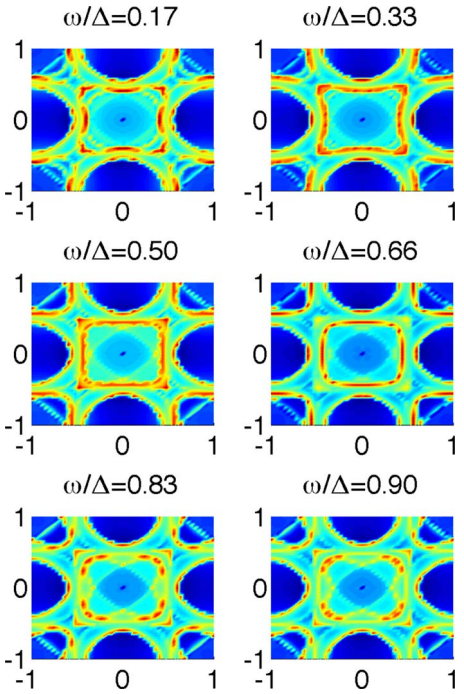

FIG. 5. (Color online) Same as Fig. 2 but for the pure SDW phase with $M=0.5t$. The results are shown for the same energies as in Fig. 2 (with $\Delta=0.3t$).

ing the expected lack of particle-hole symmetry for this phase.

In Fig. 5 we show typical QPI maps in the pure SDW phase (the results are shown for the same energies as in Fig. 2 in order to readily identify SDW features of the corresponding QPI maps in the coexisting phase studied in Sec. V). The QPI images are dominated by arcs of scattering intensity rather than spots. Distinct, isolated scattering wave vectors do not occur in the pure SDW because of the different coherence factors in this phase. As discussed in Ref. 12 in the case of intranodal scattering, the origin of peaks in the QPI maps in the pure dSC phase is caused by the dSC coherence factors which conspire to enhance the weight near the tips of the CCE, resulting in a significant enhancement of the QPI response localized near $\mathbf{q}_7$. In the pure SDW phase, on the other hand, the coherence factors cause the weight to be evenly distributed along the CCE resulting in arclike characteristic QPI features. We stress that the momentum-resolved density of states is not the cause of this qualitative difference in the QPI maps.

Finally we note that in samples with inhomogeneous coexisting regions of dSC and SDW, one way to determine which contribution of the QPI signal originates mainly from the dSC or SDW region is to compare bias-reversed QPI maps. In the pure particle-hole symmetric dSC state the $\mathbf{q}$ spots will be located at the same momenta (although with different weight), whereas in the SDW phase the arcs in the QPI maps have dispersed, resulting in new locations of the FT-STS peaks. Since applied magnetic field[65] and Zn substitution are known to enhance incommensurate magnetism in cuprate materials, these can be used to increase the particle-hole asymmetry in the scanning tunneling spectroscopy (STS) data.

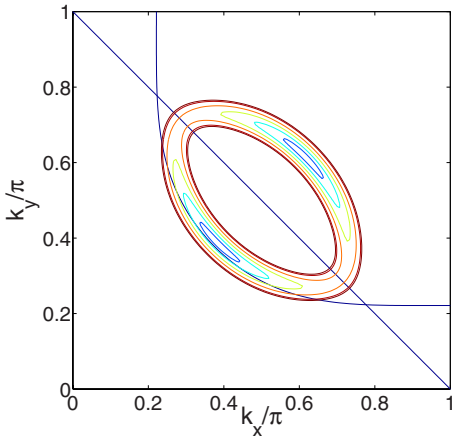

FIG. 6. (Color online) Contours of constant energy for the coexisting phase with $\Delta=0.3t$ and $M=0.5t$ plotted at the same energies ω as in Fig. 1. The contours reach the RBZ boundary when $\omega=\Delta_0=0.61\Delta$ for $M=0.5t$.

V. COEXISTING SUPERCONDUCTING AND SPIN-DENSITY WAVE PHASES

In the homogeneous coexisting state (SDW+dSC) with $\Delta\neq 0$ and $M\neq 0$, the d-wave gap collapses the arcs of spectral intensity at the Fermi level shown in Figs. 4(a) and 4(b) to nodal points. This robustness of the nodal points to SDW order away from half filling follows directly from the fact that the (π,π) ordering vector does not nest the nodal points.[74] Some representative CCEs for the coexisting phase are shown in Fig. 6. At low energies the CCEs are again reminiscent of dispersing bananas, but now shifted off the normal-state Fermi surface and exist also in the shadow band outside the RBZ. This implies the existence of shadow QPI peaks in the FT-STS response.

Once the banana tips reach the RBZ boundary, the CCEs become similar to the pure SDW case. In Fig. 7 we show the results of the QPI patterns in the coexisting phase. This figure can be directly compared to Fig. 2. We clearly see the mixing of the SDW and dSC QPI features and the importance of the crossover scale set by the energy Δ_0 where the CCE reaches the RBZ boundary: at $\omega<\Delta_0(\omega>\Delta_0)$ the QPI is dominated by the pure dSC (SDW) phase with the addition of possible shadow band features resulting from scattering involving the bananas outside the RBZ. Shadow band QPI features would be a clear signature of competing phase, but we find that the coherence factors tend to strongly suppress these peaks compared to the conventional peaks of the octet model (Fig. 1). In addition, at least for BSCCO, it seems likely that the disorder is simply too strong for these additional peaks to be observed (see Sec. VI). In Fig. 7 we have circled the position of the $\mathbf{q}_7$ peak from the pure dSC phase (see also Fig. 2). This peak appears to be extinguished when crossing the SDW zone boundary at $\omega=\Delta_0$. For the band parameter and superconducting gap $\Delta=0.3t$ used in this paper, we have $\Delta_0=0.61\Delta$ for $M=0.5t$ and $\Delta_0=0.4\Delta$ for $M=t$.

We end this section by a discussion of the momentum-summed density of states (DOS) $N(\omega)$ in the pure SDW +dSC phase given by

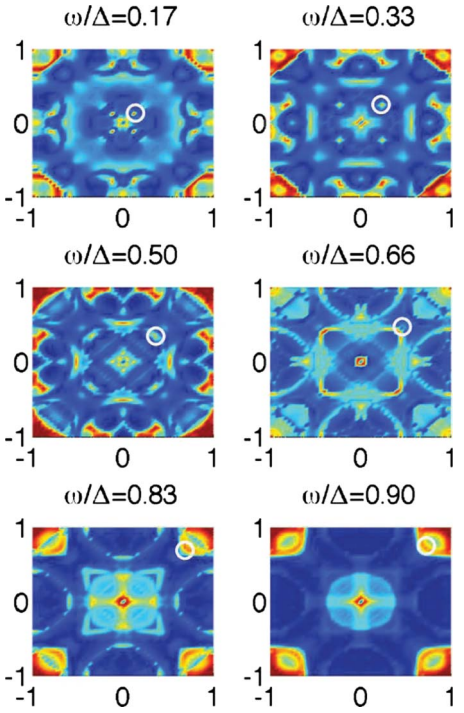

FIG. 7. (Color online) QPI maps vs q_x/π and q_y/π in the coexisting SDW+dSC phase ($\Delta=0.3t$ and $M=0.5t$) in the presence of single pointlike nonmagnetic impurity. This figure can be directly compared to Fig. 2. Note the disappearance of the spotlike feature corresponding to octet vector $\mathbf{q}_7$ above the critical energy $\Delta_0=0.61\Delta$.

$$N(\omega) = -\frac{1}{4\pi}\mathrm{Im}\sum_{i=1}^{4}\sum_{\mathbf{k}\in\mathrm{RBZ}} G_0(\mathbf{k}, s_i\omega + i\eta)_{ii}. \qquad (14)$$

As the CCEs in Fig. 6 cross the RBZ boundary they qualitatively change from banana-shaped to closed rings and one would expect a feature in the DOS at the energy Δ_0. Figure 8 shows that this is indeed the case by comparing the d-wave gap in the pure dSC phase with the SDW+dSC phase for different values of M. As the competing order is enhanced, Δ_0 is lowered and strong modifications to the conventional V-shaped d-wave superconducting gap are revealed by a peak in the DOS near $\omega=\Delta_0$. We stress that the results shown in Fig. 8 are for moderate values of M in the sense that the SDW does not produce a full gap in the DOS [as is the case for larger values of M (see, e.g., Ref. 52)].

VI. EFFECTS OF DISORDER

Above the discussion focused on pure phases, dSC, SDW, and SDW+dSC, possibly in the presence of a single pointlike nonmagnetic impurity. For a more realistic description of the underdoped cuprates this should be extended to describe QPI in a disordered short-range SDW cluster glass phase. One way to model short-range SDW correlations is by assuming a Lorentzian probability distribution p_Q of the ordering vector $\mathbf{Q}$, peaked at (π,π) with a broadening given by ξ_{SDW}^{-1}, the inverse of the SDW correlation length. The main effects of disordering with such a distribution were

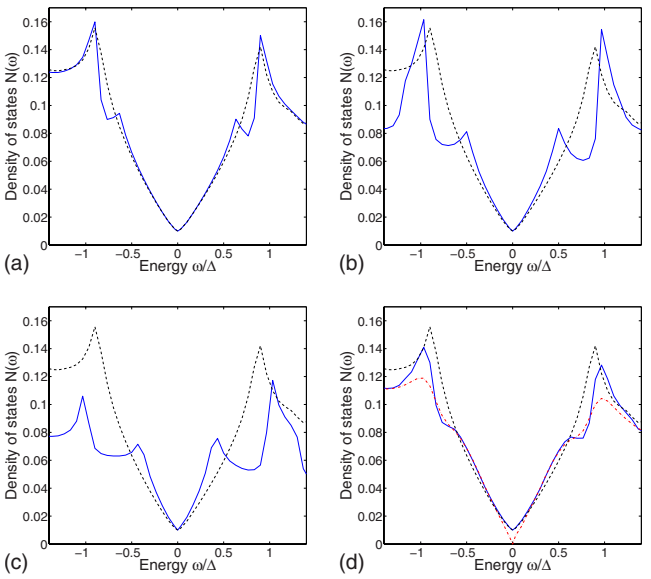

FIG. 8. (Color online) Density of states $N(\omega)$ in the coexisting SDW+dSC phase with (a) $M=0.4t$, (b) $M=0.8t$, (c) $M=t$, and (d) M averaged. In all panels the dashed (black) line shows the DOS in the pure dSC phase whereas the solid (blue) line displays the DOS in the SDW+dSC phase. In (d) the dash-dotted (red) line shows the M-averaged result for a case with a linear inelastic-scattering rate $\alpha|\omega|$ ($\alpha=0.15t$, c.f. Ref. 67) used instead of η in Eq. (14), resulting in a smoother DOS kink.

studied for the SDW phase in Ref. 73: only the part of the hole pockets which lie outside the RBZ is shifted. However, modeling the disorder by a p_Q distribution appears questionable for the CSG phase since it does not properly treat the spatial inhomogeneity of the spin glass and misses, e.g., additional low energy states existing at the boundary regions between magnetic and superconducting domains.[75] Therefore, it would be interesting to compare to quasiparticle interference patterns from more realistic real-space disorder configurations similar to those produced in Refs. 51–54, 56, 59, and 60.

An important feature of such inhomogeneous disorder studies is the spatial variation of the competing SDW order parameter M.[51–54,56] Within the present approach we can explore the effect of a distribution of M by averaging our results with respect to M. Figure 8(d) shows the DOS M averaged by a flat distribution with $M\in[0,t]$. We have also explored Gaussian distributions and found similar results. Most importantly, we have restricted the M distribution to the weak regime where no full SDW gap is generated in the DOS in agreement with experiments. As seen from Fig. 8(d), the main effect of the averaging is to transform the peak at Δ_0 into a kink in the high-energy region of the d-wave superconducting gap. We suggest that this is the origin of a similar kink seen by Alldredge *et al.*[67] in the DOS of underdoped BSCCO.

We end by discussing the effects of M averaging on the QPI patterns. Figure 9 shows the CCEs at fixed energy ω for different values for the SDW order parameter M. With M restricted to the regime $M\in[0,t]$ there is a qualitative difference between low- and high-energy CCEs as seen by

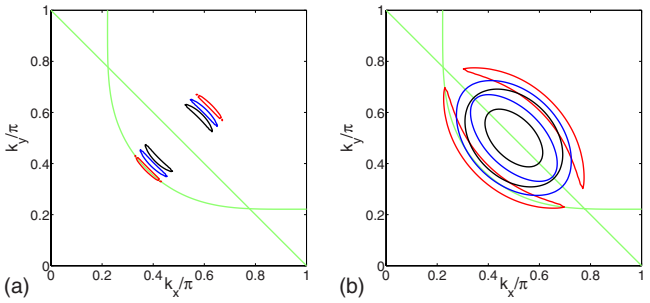

FIG. 9. (Color online) CCEs for the coexisting phase at (a) $\omega/\Delta=0.17$ and (b) $\omega/\Delta=0.66$ at $M=0$ (red), $M=0.75t$ (blue), and $M=t$ (black).

comparing Figs. 9(a) and 9(b). In the former case the CCEs are shifted but remains of the banana-type shape, whereas the latter crosses over from dSC-like to SDW-like as M increases. This will have the main effect that for low energies the M-averaged QPI maps of the coexisting phase closely resemble the dSC QPI maps. At higher energies, however, the M averaging causes a further suppression of QPI features. This point can be seen in Fig. 10 where we plot the QPI maps for the same energies as in Fig. 9; $\omega/\Delta=0.17$ (left column) and $\omega/\Delta=0.66$ (right column). The images in the top (middle) row show the QPI maps for the dSC (SDW +dSC) phase and are identical to the respective plots found in Fig. 2 (Fig. 7). The bottom row shows the M-averaged QPI maps again using a flat distribution ($M\in[0,t]$). As is evident, the low energy QPI map is virtually identical to the pure dSC result (bottom left) whereas any characteristic QPI features at higher energies $\omega>\Delta_0$ are wiped out.

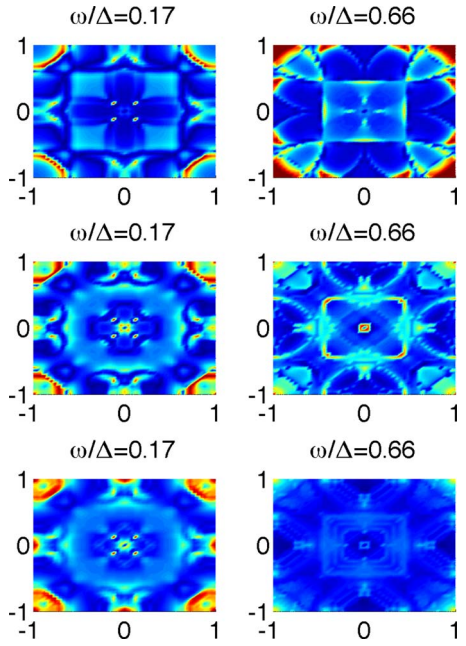

FIG. 10. (Color online) QPI maps at $\omega/\Delta=0.17$ (left column) and $\omega/\Delta=0.66$ (right column) for the dSC phase (top), coexisting phase with $M=0.5t$ (middle), and M-averaged case (bottom). The middle and bottom panels are all plotted on the same false color scale.

This effect is also seen in Fig. 11 showing the nodal and antinodal line cuts with the solid black (dashed red) lines at energies below (above) the scale set by Δ_0. By comparison to Fig. 3, the resemblance to the dSC is clear for $\omega<\Delta_0$. At $\omega>\Delta_0$, there are no peaks at the octet vectors and the line cuts become featureless. Experimentally this region of energies is characterized by dispersionless peaks along the antinodal regions. We believe this may be related to additional concomitant charge order existing in the stripe phase, which naturally leads to nondispersive QPI peaks.[13]

VII. CONCLUSIONS

We have studied quasiparticle interference phenomena in a dSC phase with coexisting SDW order potentially relevant for the cluster spin glass phase of underdoped cuprates. We have assumed that much of the qualitative physics may be captured by studying the problem with long-range SDW order. In particular, we have calculated the QPI patterns arising from scattering from a single pointlike impurity in the case of a pure metallic SDW phase and a coexisting phase of both SDW and dSC order. Due to different coherence factors in the SDW and dSC phases, the QPI maps are dominated by peaks (arcs) in the dSC (SDW) phase, respectively. In the case with coexisting order, low energy quasiparticles propagate on contours which resemble the pure superconductor, so dispersive, localized interference spots similar to those predicted by the octet model for the pure dSC system are recovered. When the tips of these contours reach the RBZ boundary, however, the contours change abruptly to those characteristic of the pure SDW and the dispersing localized interference peaks are then extinguished, as reported by Kohsaka *et al.*[36] We showed that averaging with respect to the SDW order parameter M tends to further smear only the QPI features at $\omega>\Delta_0$ in the coexisting phase.

The net result is a system where the low energy quasiparticle interference features resemble those of the optimally doped superconducting samples, namely, they disperse according to the octet model. For energies above the critical energy Δ_0, these localized spotlike features in momentum space effectively disappear, as seen in experiment.[36] Although the formation of SDW long-range order itself may be viewed as a coherent multiple-scattering process, we see from the study of the coexisting SDW+dSC system that the quasiparticle states near the antinode are not destroyed by broadening in this process, but simply folded back. Thus in the realistic situation with short-range SDW order, some scatterings from spin modulations will occur, but still well-defined quasiparticle peaks should remain as seen in ARPES measurements.[1,43,44] This resolves an apparent paradox in the comparison of the two experimental techniques in their view of the antinodal quasiparticles. It is the localized QPI **q**-space structures due to these states which are destroyed and not the states themselves.

A prediction of the present SDW+dSC scenario arises for samples (presumably in the overdoped regime) without FT-STS extinction lines. In that case one should be able to induce the competing order by magnetic field[65] or, e.g., Zn substitution and hence observe a concomitant induced ex-

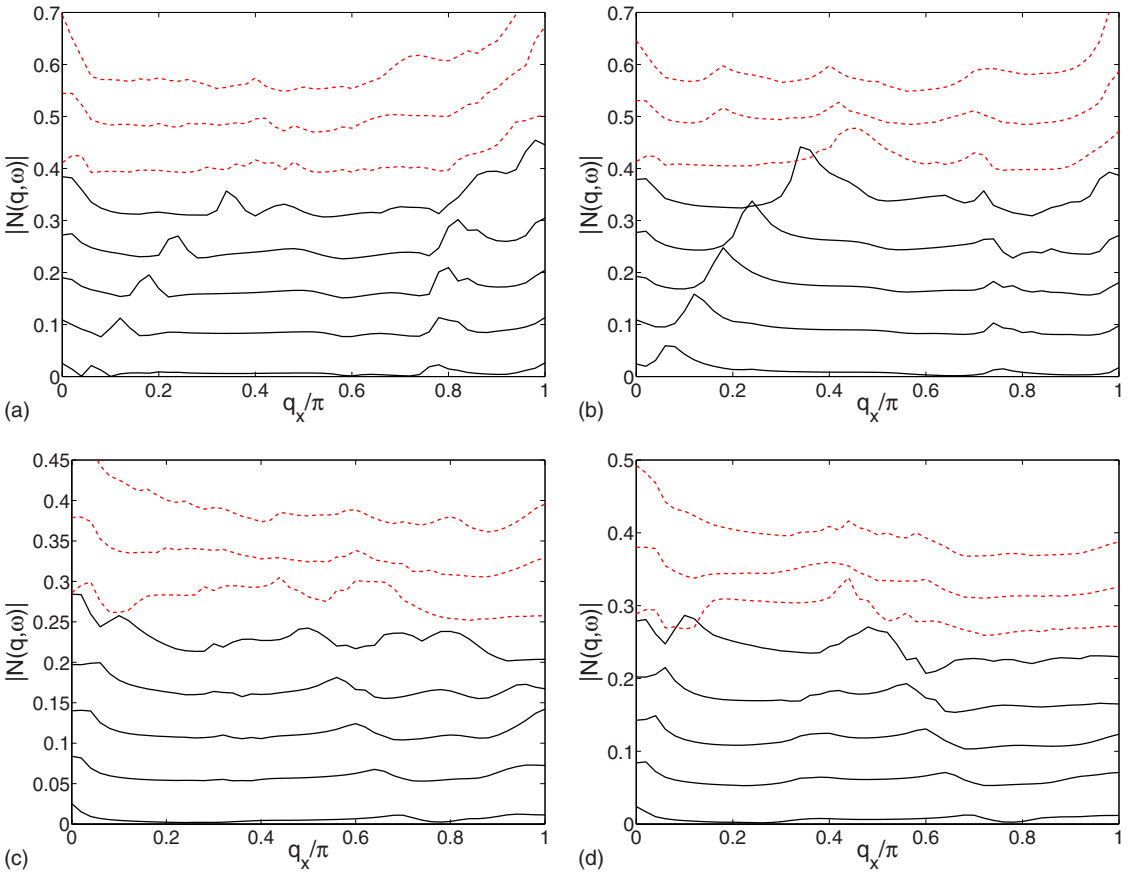

FIG. 11. (Color online) QPI line cuts at the same energies as in Figs. 3 along the [(a) and (b)] (110) and [(c) and (d)] (100) directions for the coexisting SDW+dSC phase with $\Delta=0.3t$ and M averaged over a flat distribution with $M\in[0,t]$. The line cuts at energies above the crossover $\omega=\Delta_0$ are indicated by red dashed lines. The curves are displaced similarly to Fig. 3.

tinction line in the QPI maps and kinks at the corresponding energy in the DOS.

We emphasize that the formalism presented in this paper is essentially identical for any competing order scenario with ordering wave vector near (π,π). We believe that the bulk of the experimental evidence supports the identification of the competing phase with short-range incommensurate SDW order or quasistatic fluctuations from incipient order, as observed in μSR. We have therefore discussed the extinction of QPI above a critical energy in this context, but other explanations with a similar structure may be possible.

Finally, we stress that a quantitative understanding of the QPI patterns requires a more sophisticated description of disorder than that adopted here. It is thought that the potential produced by a single defect has components in at least the screened Coulomb and pairing channels and some accounts of the latter are known to be necessary to reproduce the correlations between dopant position and gap size observed in the BSCCO system.[17] We have neglected these details here, but they are discussed, e.g., in Ref. 19. Nevertheless, the patterns produced by our single potential scatterer were found to be sufficient to describe the basic phenomenology of Kohsaka *et al.*[36] for the octet $\mathbf{q}_7$ peak. It will be interesting to see if more sophisticated simulations can also reproduce the behavior of the other octet vectors and their weights correctly.[68]

One aspect of the current picture which remains unclear is the extent to which static order is required. The QPI extinction phenomenon observed by Kohsaka *et al.*[36] is observed in BSCCO samples with doping levels of 6–19 %, i.e., including optimal doping where recent neutron experiments have claimed a 32 meV spin gap.[76] Still, near (π,π), some intensities remain below this energy and μSR continues to indicate frozen magnetic order even in these samples at low temperatures.[48] It may be that the magnetism in this system is simply too disordered to be seen by current neutron experiments or that fluctuating order, slow on the time scale of these experiments, is sufficient to create the effects we describe here. A more sophisticated treatment of short-range order is required to address these questions.

ACKNOWLEDGMENTS

The authors acknowledge valuable discussions with J. W. Alldredge, J. C. Davis, Z.-X. Shen, and M. Vojta. B.M.A. acknowledges support from the Villum Kann Rasmussen Foundation and P.J.H. from DOE-BES under Contract No. DE-FG02-05ER46236.

[1] A. Damascelli, Z. Hussain, and Z.-X. Shen, Rev. Mod. Phys. **75**, 473 (2003).
[2] H. Fu and D. H. Lee, Phys. Rev. B **74**, 174513 (2006).
[3] J. E. Hoffman, K. McElroy, D.-H. Lee, K. M. Lang, H. Eisaki, S. Uchida, and J. C. Davis, Science **297**, 1148 (2002).
[4] C. Howald, H. Eisaki, N. Kaneko, M. Greven, and A. Kapitulnik, Phys. Rev. B **67**, 014533 (2003).
[5] K. McElroy, R. W. Simmonds, J. E. Hoffman, D.-H. Lee, J. Orenstein, H. Eisaki, S. Uchida, and J. C. Davis, Nature (London) **422**, 592 (2003).
[6] M. Vershinin, S. Misra, S. Ono, Y. Abe, Y. Ando, and A. Yazdani, Science **303**, 1995 (2004).
[7] K. McElroy, D.-H. Lee, J. E. Hoffman, K. M. Lang, J. Lee, E. W. Hudson, H. Eisaki, S. Uchida, and J. C. Davis, Phys. Rev. Lett. **94**, 197005 (2005).
[8] A. Hashimoto, N. Momono, M. Oda, and M. Ido, Phys. Rev. B **74**, 064508 (2006).
[9] Q. H. Wang and D. H. Lee, Phys. Rev. B **67**, 020511(R) (2003).
[10] P. T. Sprunger, L. Petersen, E. W. Plummer, E. Lægsgaard, and F. Besenbacher, Science **275**, 1764 (1997).
[11] D. Zhang and C. S. Ting, Phys. Rev. B **67**, 100506(R) (2003).
[12] T. Pereg-Barnea and M. Franz, Phys. Rev. B **68**, 180506(R) (2003).
[13] L. Capriotti, D. J. Scalapino, and R. D. Sedgewick, Phys. Rev. B **68**, 014508 (2003).
[14] L. Zhu, W. A. Atkinson, and P. J. Hirschfeld, Phys. Rev. B **69**, 060503(R) (2004).
[15] S. Misra, M. Vershinin, P. Phillips, and A. Yazdani, Phys. Rev. B **70**, 220503(R) (2004).
[16] K. McElroy, J. Lee, J. A. Slezak, D.-H. Lee, H. Eisaki, S. Uchida, and J. C. Davis, Science **309**, 1048 (2005).
[17] T. S. Nunner, B. M. Andersen, A. Melikyan, and P. J. Hirschfeld, Phys. Rev. Lett. **95**, 177003 (2005).
[18] B. M. Andersen, A. Melikyan, T. S. Nunner, and P. J. Hirschfeld, Phys. Rev. B **74**, 060501(R) (2006).
[19] T. S. Nunner, W. Chen, B. M. Andersen, A. Melikyan, and P. J. Hirschfeld, Phys. Rev. B **73**, 104511 (2006).
[20] L. Dell'Anna, J. Lorenzana, M. Capone, C. Castellani, and M. Grilli, Phys. Rev. B **71**, 064518 (2005).
[21] M. Cheng and W. P. Su, Phys. Rev. B **72**, 094512 (2005).
[22] Y. H. Liu, K. Takeyama, T. Kurosawa, N. Momono, M. Oda, and M. Ido, Phys. Rev. B **75**, 212507 (2007).
[23] T. Hanaguri, C. Lupien, Y. Kohsaka, D.-H. Lee, M. Azuma, M. Takano, H. Takagi, and J. C. Davis, Nature (London) **430**, 1001 (2004).
[24] W. D. Wise, M. C. Boyer, K. Chatterjee, T. Kondo, T. Takeuchi, H. Ikuta, Y. Wang, and E. W. Hudson, Nat. Phys. **4**, 696 (2008).
[25] A. Polkovnikov, M. Vojta, and S. Sachdev, Phys. Rev. B **65**, 220509(R) (2002); Physica C **388-389**, 19 (2003).
[26] C. T. Chen and N. C. Yeh, Phys. Rev. B **68**, 220505(R) (2003).
[27] D. Podolsky, E. Demler, K. Damle, and B. I. Halperin, Phys. Rev. B **67**, 094514 (2003).
[28] B. M. Andersen, P. Hedegard, and H. Bruus, Phys. Rev. B **67**, 134528 (2003).
[29] L. Udby, B. M. Andersen, and P. Hedegård, Phys. Rev. B **73**, 224510 (2006).
[30] J.-X. Li, C.-Q. Wu, and D.-H. Lee, Phys. Rev. B **74**, 184515 (2006).
[31] S. E. Brown, E. Fradkin, and S. A. Kivelson, Phys. Rev. B **71**, 224512 (2005).
[32] A. Ghosal, A. Kopp, and S. Chakravarty, Phys. Rev. B **72**, 220502(R) (2005).
[33] U. Chatterjee, M. Shi, A. Kaminski, A. Kanigel, H. M. Fretwell, K. Terashima, T. Takahashi, S. Rosenkranz, Z. Z. Li, H. Raffy, A. Santander-Syro, K. Kadowaki, M. R. Norman, M. Randeria, and J. C. Campuzano, Phys. Rev. Lett. **96**, 107006 (2006).
[34] E. Bascones and B. Valenzuela, Phys. Rev. B **77**, 024527 (2008).
[35] T. Hanaguri, Y. Kohsaka, J. C. Davis, C. Lupien, I. Yamada, M. Azuma, M. Takano, K. Ohishi, M. Ono, and H. Takagi, Nat. Phys. **3**, 865 (2007).
[36] Y. Kohsaka, C. Taylor, P. Wahl, A. Schmidt, J. Lee, K. Fujita, J. Alldredge, J. Lee, K. McElroy, H. Eisaki, S. Uchida, D.-H. Lee, and J. C. Davis, Nature (London) **454**, 1072 (2008).
[37] T. Hanaguri, Y. Kohsaka, M. Ono, M. Maltseva, P. Coleman, I. Yamada, M. Azuma, M. Takano, K. Ohishi, and H. Takagi, Science **323**, 923 (2009).
[38] S. Graser, P. J. Hirschfeld, and D. J. Scalapino, Phys. Rev. B **77**, 184504 (2008).
[39] M. Eschrig, Adv. Phys. **55**, 47 (2006).
[40] T. Dahm and L. Tewordt, Phys. Rev. Lett. **74**, 793 (1995).
[41] S. M. Quinlan, P. J. Hirschfeld, and D. J. Scalapino, Phys. Rev. B **53**, 8575 (1996).
[42] T. Dahm, P. J. Hirschfeld, D. J. Scalapino, and L.-Y. Zhu, Phys. Rev. B **72**, 214512 (2005).
[43] J. C. Campuzano, H. Ding, M. R. Norman, H. M. Fretwell, M. Randeria, A. Kaminski, J. Mesot, T. Takeuchi, T. Sato, T. Yokoya, T. Takahashi, T. Mochiku, K. Kadowaki, P. Guptasarma, D. G. Hinks, Z. Konstantinovic, Z. Z. Li, and H. Raffy, Phys. Rev. Lett. **83**, 3709 (1999).
[44] M. Shi, A. Bendounan, E. Razzoli, S. Rosenkranz, M. R. Norman, J. C. Campuzano, J. Chang, M. Mansson, Y. Sassa, T. Claesson, O. Tjernberg, L. Patthey, N. Momono, M. Oda, M. Ido, S. Guerrero, C. Mudry, and J. Mesot, arXiv:0810.0292 (unpublished).
[45] J. Tranquada, in *Handbook of High Temperature Superconductivity: Theory and Experiment*, edited by J. R. Schrieffer and J. S. Brooks (Springer-Verlag, Berlin, 2007).
[46] M. Fujita, H. Goka, K. Yamada, J. M. Tranquada, and L. P. Regnault, Phys. Rev. B **70**, 104517 (2004).
[47] M.-H. Julien, Physica B **329-333**, 693 (2003).
[48] C. Panagopoulos, J. L. Tallon, B. D. Rainford, J. R. Cooper, C. A. Scott, and T. Xiang, Solid State Commun. **126**, 47 (2003).
[49] X. J. Zhou, T. Yoshida, D.-H. Lee, W. L. Yang, V. Brouet, F. Zhou, W. X. Ti, J. W. Xiong, Z. X. Zhao, T. Sasagawa, T. Kakeshita, H. Eisaki, S. Uchida, A. Fujimori, Z. Hussain, and Z.-X. Shen, Phys. Rev. Lett. **92**, 187001 (2004).
[50] S. A. Kivelson, I. P. Bindloss, E. Fradkin, V. Oganesyan, J. M. Tranquada, A. Kapitulnik, and C. Howald, Rev. Mod. Phys. **75**, 1201 (2003).
[51] G. Alvarez, M. Mayr, A. Moreo, and E. Dagotto, Phys. Rev. B **71**, 014514 (2005); M. Mayr, G. Alvarez, A. Moreo, and E. Dagotto, *ibid.* **73**, 014509 (2006).
[52] W. A. Atkinson, Phys. Rev. B **71**, 024516 (2005).
[53] J. A. Robertson, S. A. Kivelson, E. Fradkin, A. C. Fang, and A. Kapitulnik, Phys. Rev. B **74**, 134507 (2006).
[54] A. Del Maestro, B. Rosenow, and S. Sachdev, Phys. Rev. B **74**, 024520 (2006).
[55] M. Vojta, T. Vojta, and R. K. Kaul, Phys. Rev. Lett. **97**, 097001 (2006).
[56] B. M. Andersen, P. J. Hirschfeld, A. P. Kampf, and M. Schmid,

Phys. Rev. Lett. **99**, 147002 (2007).
[57] H. Alloul, J. Bobroff, M. Gabay, and P. J. Hirschfeld, Rev. Mod. Phys. **81**, 45 (2009).
[58] W. A. Atkinson, Phys. Rev. B **75**, 024510 (2007).
[59] B. M. Andersen and P. J. Hirschfeld, Phys. Rev. Lett. **100**, 257003 (2008).
[60] G. Alvarez and E. Dagotto, Phys. Rev. Lett. **101**, 177001 (2008).
[61] B. M. Andersen and P. J. Hirschfeld, Physica C **460–462**, 744 (2007).
[62] C. Li, S. Zhou, and Z. Wang, Phys. Rev. B **73**, 060501(R) (2006).
[63] K. Seo, H. D. Chen, and J. Hu, Phys. Rev. B **76**, 020511(R) (2007); **78**, 094510 (2008).
[64] M. Vojta and O. Rösch, Phys. Rev. B **77**, 094504 (2008).
[65] B. Lake, H. M. Rønnow, N. B. Christensen, G. Aeppli, K. Lefmann, D. F. McMorrow, P. Vorderwisch, P. Smeibidl, N. Mangkorntong, T. Sasagawa, M. Nohara, H. Takagi, and T. E. Mason, Nature (London) **415**, 299 (2002).
[66] T. Das, R. S. Markiewicz, and A. Bansil, Phys. Rev. B **77**, 134516 (2008).
[67] J. W. Alldredge, J. Lee, K. McElroy, M. Wang, K. Fujita, Y. Kohsaka, C. Taylor, H. Eisaki, S. Uchida, P. J. Hirschfeld, and J. C. Davis, Nat. Phys. **4**, 319 (2008).
[68] B. M. Andersen and P. J. Hirschfeld (unpublished).
[69] C. Bena, S. Chakravarty, J. Hu, and C. Nayak, Phys. Rev. B **69**, 134517 (2004).
[70] A. V. Balatsky, I. Vekhter, and J.-X. Zhu, Rev. Mod. Phys. **78**, 373 (2006).
[71] B. M. Andersen, S. Graser, and P. J. Hirschfeld, Phys. Rev. B **78**, 134502 (2008).
[72] S. Chakravarty, C. Nayak, and S. Tewari, Phys. Rev. B **68**, 100504(R) (2003).
[73] N. Harrison, R. D. McDonald, and J. Singleton, Phys. Rev. Lett. **99**, 206406 (2007).
[74] E. Berg, C.-C. Chen, and S. A. Kivelson, Phys. Rev. Lett. **100**, 027003 (2008).
[75] B. M. Andersen, I. V. Bobkova, P. J. Hirschfeld, and Yu. S. Barash, Phys. Rev. B **72**, 184510 (2005).
[76] B. Fauqué, Y. Sidis, L. Capogna, A. Ivanov, K. Hradil, C. Ulrich, A. I. Rykov, B. Keimer, and P. Bourges, Phys. Rev. B **76**, 214512 (2007).
[77] B. M. Andersen and P. Hedegard, Phys. Rev. Lett. **95**, 037002 (2005).